JOURNAL OF NANO AND MATERIALS SCIENCE RESEARCH
Volume 3, No.2 (Special Issue, 2025), pp. 44 – 49
Available online at journals.nanotechunn.com/jnmsr

ORIGINAL ARTICLE

Investigating the Morphology and Dielectric Characteristics of Copper-Zinc-Iron Sulphide Nano-Films for Electronic Applications

Joseph O. Emegha[a,*], *Chukwunwike Ossai*[b], *Temitope Plasile Fowodu*[c]

[a]*Department of Physics, Hensard University, Toru Orua, Bayelsa State, Nigeria.*
[b]*Department of Physics, Dennis Osadebay University, Anwai, Asaba, Delta State, Nigeria.*
[c]*Tai Solarin University of Education, Ijagun, P.M.B 2118, Ijebu-Ode, Ogun State, Nigeria.*

KEYWORDS

Band gap, Deposition, Optical, Thin film, Wavelength

ARTICLE HISTORY

Received: December 22, 2024
Revised: June 18, 2025
Accepted: June 24, 2025
Published: February 13, 2026

ABSTRACT

This study examined the deposition of copper zinc iron sulphide (CZFS) thin films on glass substrates at ambient temperature using the chemical bath deposition (CBD) method. The deposited CZFS thin films were analyzed employing transmission electron microscopy (TEM) and UV-visible spectroscopy. Morphological analyses demonstrated that the CZFS films deposited over different durations exhibited crystallization with varying grain structures. The optical properties, such as the imaginary and real parts of the dielectric constant, loss angle, surface energy loss function (SELF), and volume energy loss function (VELF), were computed using UV-Vis spectroscopic data. Furthermore, the band gap was ascertained through absorption spectrum fitting (ASF). The band gap of the material varied from 0.99 to 1.55 eV, corresponding to increasing deposition durations of the films. These results suggest that the chemical bath deposited CZFS films can be engineered for a range of electronic applications.

1 Introduction

Quaternary thin films (TFs) of copper, iron, and zinc sulphide have been extensively researched due to their semiconductor characteristics [1], [2]. The structural and physical characteristics of the quaternary copper-zinc-iron-sulphide TFs have been thoroughly examined [3]. Numerous studies have also focused on the physical properties of ternary systems such as copper-zinc-sulphide [4] – [7], copper-iron-sulphide [8], [9], and zinc-iron-sulphide thin films [10], [11], including their binary components like copper sulphide, zinc sulphide, and iron sulphides [12] – [14].

Copper sulphide (CuS) demonstrates promising applications in solar energy conversion, catalysis, and sensing technologies [12], [15]. Over the past few decades, CuS has garnered significant attention as an important semiconductor due to its exceptional optical, electronic, and other physical and chemical characteristics. Specifically, it functions as a p-type semiconducting material with a band gap of 2.37 eV [12]. Its complex structures and valence states give rise to distinct properties and offer potential applications in various fields including solar cells, optical filters superconductors, chemical sensors, and photocatalysis [9].

Zinc sulphide (ZnS) is a fascinating semiconductor substance with a broad energy gap that has attracted considerable attention due to its potential applications in optoelectronic devices, such as solar cells and anti-reflective coating layers [13], [16]. Among different types of sulphides, zinc sulphide has been extensively researched from both practical and theoretical perspectives because of its distinctive physical properties [13]. Iron sulphide (FeS) thin film is considered a promising option for the fabrication of solar cells due to its impressive band gap energy, which falls within the range of 1 to 2 eV [14]. Additionally, iron sulphide thin films have garnered significant interest from researchers for their potential in photovoltaic and photo-electrochemical applications [17].

Notably, the quaternary material of copper-zinc-iron sulphide (CZFS) thin films are composed of readily available non-toxic

* **CORRESPONDING AUTHOR** | Joseph O. Emegha, ✉ dr.emegha@hensarduniversity.edu.ng

elements that are abundant in nature [9]. A modification in the structure of this material can influence its optical absorption because it may alter the band structure, carrier density, and electronic transitions. These alterations play a critical role in shaping the optical properties of the TFs for devices application [3], [6]. Thus, comprehending these nano-structural features is essential for creating efficient approaches to enhance the optical characteristics of nanomaterials and design novel optical devices [3].

Analyzing the optical absorption, especially the shape and shift of the absorption edge, is a highly useful approach for understanding the fundamental process of optically-driven transitions in both crystalline and amorphous materials. It also offers insights into the energy band structure [18], [19]. Recently, some researchers have examined the elemental, optical and electrical properties of TFs made of CZFS [3].

However, knowledge regarding their transmission electron microscope (TEM) and solid-state properties remains limited. Therefore, this study aims to achieve two main objectives: first, to investigate the morphological properties of CZFS thin films using TEM, and second, to assess the impact of deposition time on their solid-state characteristics using a cost-effective CBD method at room temperature [9]. Finally, the suitability of these films for optoelectronic applications was evaluated.

2 Experimental Details

2.1 Synthesis and Characterization of CZFS TFs

Using a CBD approach, the CZFS TFs were deposited on glass substrates at room temperature. Copper (II) chloride dehydrate, Iron (III) chloride, zinc chloride, and thiourea make up the reactive solution. A recently published study by Emegha et al., [3] highlights specifics of the growth processes. The samples were designated as C1, C2, and C3 according to the reaction durations of 12, 15, and 18 hours [3].

The morphology of the films was investigated using transmission electron microscopy with a TECNAI F20 instrument. The optical properties were measured across the wavelength range of 300 to 900 nm using a UV-1800 spectrophotometer. Prior to collecting the absorption data, a clean substrate was employed as the reference. After establishing the baseline, the thin film samples were positioned vertically on the sample holder and exposed to monochromatic illumination. The acquired absorption data were then used to calculate other optical parameters, including band gap, real and imaginary dielectric constants, loss angle, volume energy loss function (VELF) and surface energy loss function (SELF).

3 Results and Discussions

3.1 Surface and Compositional analysis of CZFS TFs

Figure 1 depicts the TEM micrographs of CZFS thin film samples deposited over various time periods. The images show well-packed nanoparticles of various sizes and shapes in granular form. It was observed that the sizes of the grains increase with increase in deposition time. Besides shapes that are not uniform, smaller grains in isolation are also visible within the films.

Figure 1a shows nano-grains with partial density and compactness form on some parts of the substrates in C1. With increased deposition time, the nanoparticles increase in size as they aggregate into larger grains, as illustrated in Figure 1b for C2. After 18 hours (Figure 1c), these larger grain clusters transform into a substantial amount of roughly spherical grains resembling individual grains.

This transformation indicates that the deposition time significantly affects the formation and characteristics of the nano-grains The primary explanation is that the deposition time improves the roughness of the crystalline grains and reduces defects in the CZFS structures [20]. This uneven morphology proves advantageous for photovoltaic manufacturing, as it attracts a greater number of photons, thereby increasing absorption and current densities within the deposited TFs system [3].

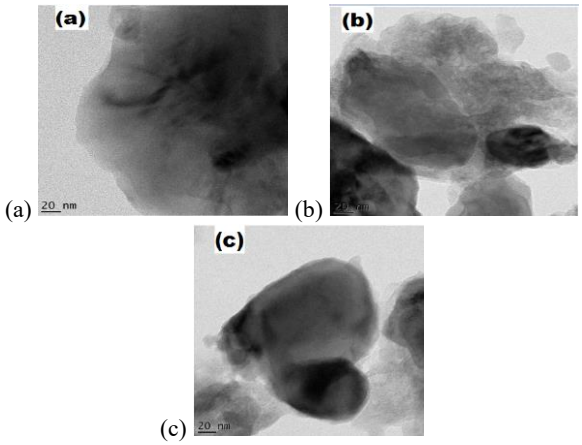

Figure 1: TEM images of CZFS TFs of (a) C1, (b) C2 and (c) C3

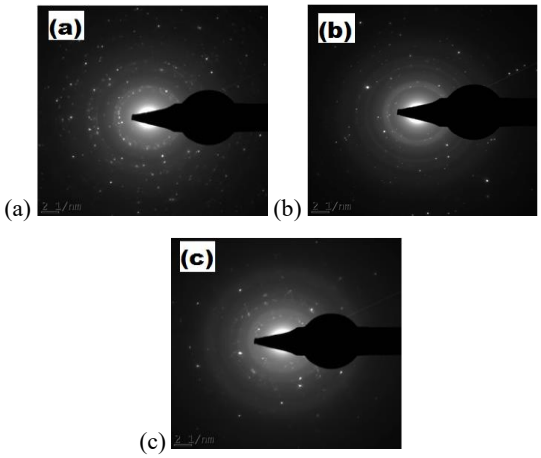

Figure 2: SAED patterns of CZFS TFs of (a) C1, (b) C2 and (c) C3

The direct bandgap of CZFS TFs was evaluated using Equation 1, which relates the absorption coefficient α(v) and the photon energy (hv) by [22], [23]:

$$\alpha(v)hv = B(hv - Eg)^n \quad (1)$$

The energy gap between the valence and conduction bands of a material is known as the optical band gap, represented by E_g. The photon energy is denoted as hv, and B is a constant related to the transition probability. Furthermore, the index n, called the power factor of the electronic transition mode, can have values ranging from 1/2 to 3, depending on the type of electronic transition within the material. Specifically, n takes the value of 1/2 for allowed direct transitions, 2 for allowed indirect transitions, 3/2 for forbidden direct transitions, and 3 for forbidden indirect transitions [22], [24]. The absorption spectrum fitting (ASF) analysis technique permits the optical band gap to be calculated using the Equation 2 [25]:

$$E_{g(ASF)} = \frac{hc}{\lambda_g} = \frac{1239.83}{\lambda_g} \quad (2)$$

where the Planck constant is represented by h, the speed of light is denoted by c, and the wavelength of the corresponding band gap is signified by λ_g. By applying the Beer-Lambert law, the Equation 1 can be rearranged to express it as a function of wavelength, as demonstrated in the Equation 3 [23], [25]:

$$A(\lambda) = K_1\lambda\left(\frac{1}{\lambda} - \frac{1}{\lambda_g}\right)^n + K_2 \quad (3)$$

The Beer-Lambert law establishes a relationship between a material's absorbance and the concentration of the absorbing species. The constants K_1 and K_2 are linked to the material's reflectance characteristics. By employing the provided Equation 3, the optical band gap of the deposited material can be determined in electron volts without taking the sample thickness into account [25]. Determination of E_g is achieved by plotting $(A/\lambda)^2$ against $(1/\lambda)$ (Figure 3). E_g can be estimated by extrapolating the linear segment of (A/λ)2 to the x-intercept. This value is then used to calculate the material's band gap using the equation E_g (ASF) = 1239.83/λg [23], [25]. According to the ASF method, the estimated band gap values for samples C1, C2, and C3 are 0.99 eV, 1.55 eV, and 1.24 eV, respectively.

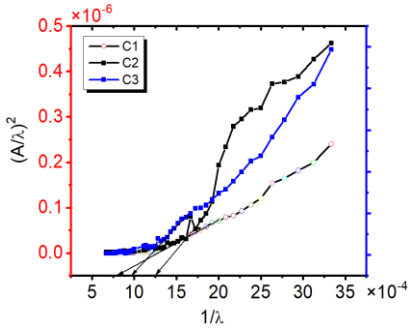

Figure 3: The ASF plot of CZFS TFs

Commonly, a variety of factors contribute to the fluctuations observed in the measured band gap values. One such factor is the inherent nature of the deposited material, which results in samples with larger grain sizes that vary depending on the deposition duration [3]. Additionally, it is proposed that the band tailing phenomenon, which arises from the disorder in the CZFS nano-system, significantly influences the variations in the band gap values [26]. The values of the deposited band gaps can be advantageous for solar cell manufacturing, as the range of the band gaps permit a greater number of photons to reach the absorbing layers and generate enhanced photocurrents [2], [27], [28].

The electronic dielectric constant (ε) of the material must be examined in order to analyze the electronic structure and density of states within the band gap of the CZFS film. One inherent characteristic of the material that defines the optical characteristics of the transparent solid is the dielectric constant [29]. Equation 4 determines the dielectric constant. [3], [30]:

$$\varepsilon = \varepsilon_r + \varepsilon_i \quad (4)$$

The imaginary part (ε_i) of the electronic dielectric constant is related to the energy dissipation brought on by the oscillation of dipoles inside the electric field, whilst the real part (ε_r) represents the speed at which the electromagnetic wave passes through the material [3], [31]. Both the extinction coefficient and the refractive index affect the real and imaginary components of the electronic dielectric constants, which may be calculated using the relations in Equations 5 and 6 below [18].

$$\varepsilon_r = n^2 - k^2 \quad (5)$$

$$\varepsilon_i = 2\pi k \quad (6)$$

Figure 4a and Figure 4b illustrate how ε_r and ε_i change with wavelength, respectively. The similarity between Samples C2 and C3 was noted. As the wavelength increases in both situations, the real dielectric constant drops off significantly. The fact that the real dielectric constants vary in value was also demonstrated by the Figure 4a. The varying deposition times and refractive indices of the various samples are the reason for this [18]. Ref. [18] reported a similar trend for thin films of chalcogenides.

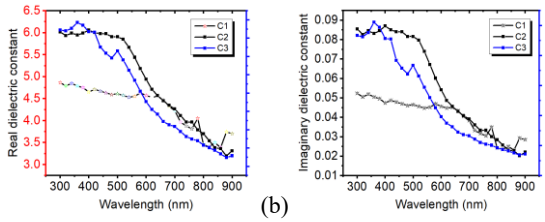

Figure 4: (a) Real (b) Imaginary dielectric constant of CZFS TFs

As the wavelength increases, the imaginary component of the dielectric constant, as shown in Figure 4b, undergoes a significant decrease from 0.09 to 0.02. This reduction in the imaginary part at higher wavelengths can be attributed to light

scattering induced by the nanometer-scale grain size of the deposited films. Furthermore, the low recombination losses and diminished interference with charge carrier transport within the material provide additional insight into this observed phenomenon [19].

The measured values of the dielectric constant can be used to determine the dielectric loss (tan ϕ). The energy dissipation of a dielectric material under an alternating electric field is associated with the tangent of the phase angle (tan φ), which can vary due to altered deposition conditions. [25], [32]. The reciprocal of the quality factor represents the "quality" or "persistence" of the oscillation, and it corresponds to the power dissipation rate of an oscillation functioning in a mechanical, electrical, or electromechanical mode within a dissipative system [30], [33].

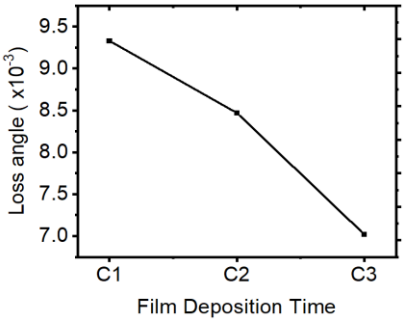

Figure 5: Relationship between loss angle and deposition time

Materials with a higher dielectric constant tend to exhibit greater dielectric loss. In addition to the material's temperature, composition, and structure, the dielectric loss is also influenced by the frequency of the applied electromagnetic field. Equations 7 and 8 were used to determine the (tan ϕ) and the loss angle (ϕ) [25], [32]:

$$tan\,\phi = \frac{\varepsilon_i}{\varepsilon_r} \quad (7)$$

$$\phi = tan^{-1}\left(\frac{\varepsilon_i}{\varepsilon_r}\right) \quad (8)$$

The loss angle of CZFS thin films exhibits a marked decline as the deposition time increases, as illustrated in Figure 5. This rapid reduction in loss angle can be attributed to the extended deposition duration. Furthermore, since the loss angle is below unity, the material is expected to exhibit minimal energy dissipation when utilized in device applications [25].

The energy loss function in the dielectric can be used to characterize the inelastic scattering of electrons on the surface [34]. Through the dielectric function, the energy loss is linked to the material's optical properties. When rapid electrons move across the material's bulk and surface, the photon energy determines the surface and volume loss functions. The real and imaginary components of the dielectric functions determine the surface energy loss function (SELF) and the volume energy loss function (VELF), and these can be computed using the relations shown in Equation 9 and 10 [34]:

$$\text{SELF} = \frac{\varepsilon_i}{(\varepsilon_{r+1})^2 + \varepsilon_i^2)} \quad (9)$$

$$\text{VELF} = \frac{\varepsilon_i}{(\varepsilon_i^2 + \varepsilon_r^2)} \quad (10)$$

Figures 6a and 6b display the variations in the SELF and VELF as a function of photon energy for CZFS TFs formed over various time periods. The plots show that both SELF and VELF values increase with increasing deposition time, which raises electron gain. The free charge carriers that move within the surface and volume of the deposited material are mostly responsible for these benefits, which show almost the same behavior [34]. Furthermore, the energy loss function in the dielectric function can be used to characterize the inelastic scattering of electrons on the surface. At a particular incident photon energy, the energy loss from volume interactions exceeds that from surface interactions. Similarly, the photon energy range corresponds to the locations of the maximum and minimum values of the volume energy loss function and surface energy loss function [32].

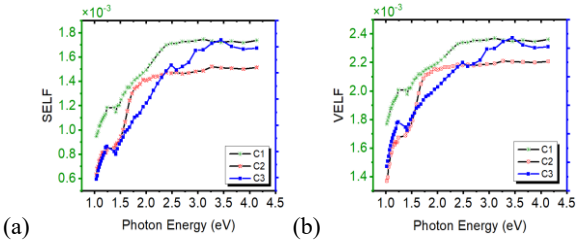

Figure 6: Relationship between (a) SELF (b) VELF and Photon Energy in CZFS TFs

Conclusion

This study examined the CBD method for depositing thin films of copper-zinc-iron sulphide on glass substrates at ambient temperature. The SAED pattern revealed that the samples possessed a crystalline structure, while TEM examination showed their morphological structure. The UV spectra of the samples were used to compute dielectric parameters, such as the loss angle, surface energy loss function, volume energy loss function, and the imaginary and real components of the dielectric constants. The findings indicate that the band gaps increased with longer deposition times, ranging from 0.99 to 1.55 eV. This suggests that extending the deposition times can enhance the CZFS TFs deposition characteristics.

Declaration of Competing Interest

The authors disclose no personal or financial conflicts that might have affected the research.

References

[1] A Ziti, B Hartiti, S Smairi, et al. Optical investigations of Cu_2BaSnS_4 quaternary nanostructure absorbers deposited by dip-coating technique. *J Mater Sci: Mater Electron* 2022; **33**, 24477–24492. https://doi.org/10.1007/s10854-022-09160-2

[2] HS Min, and T Joseph Sahaya Anand. A Review of Chalcogenide Thin Films for Solar Cell Applications. I*ndian J. Sci. Technol*. 2015; 8(12), 67499.

[3] JO Emegha, KE Ukhurebor, UO Aigbe, J Damisa and AV Babalola. Synthesis and characterization of copper zinc iron sulphide (CZFS) thin films. Heliyon 2022; 8, e10331. https://doi.org/10.1016/j.heliyon.2022.e10331

[4] CC Uhuegbu, EB Babatunde and CO Oluwafemi. The study of copper zinc sulphide (CuZnS2) thin film. Turk. J. Phys. 2008; 32, 39–47.

[5] JO Emegha, CM Okafor and KE Ukhurebor. Optical properties of copper-zinc sulphide network from mixed single solid source precursors of copper and zinc dithiocarbamate. Walaika J. Sci. & Tech. 2021; 18(9), 1-11.

[6] JO Emegha, KE Ukhurebor U Aigbe, B Olofinjana, SO Azi and MA Eleruja. Effect of deposition temperature on the properties of copper-zinc sulphide thin films using mixed copper and zinc dithiocarbamate precursors. GU J Sci. 2022; 35(4): 1556-1570. DOI: 10.35378/gujs.887025

[7] JO Emegha, B Olofinjana, KE Ukhurebor, JT Adegbite and MA Eleruja. Electrical properties of semiconducting copper zinc sulphide thin films. Curr. Appl. Sci. Technol. 2022; 22(1), 1–9.

[8] Z Shi and AH. Jayatissa. Preparation and characterization of cobalt-doped iron pyrite (FeS2) thin films. Prog Nat Sci-Mater. 2020; /doi.org/10.1016/j.pnsc.2020.03.002

[9] QA Adeniji, TO Fowodu, K Odunaike and AT Talabi. The Growth and Opto-Electrical Characterization of SILAR grown Iron Copper Sulphide (FeCuS) Ternary Thin Films. Int. J. Thin. Fil. Sci. Tec. 2021; 10(1), 7-11

[10] VN Udeajah and DU Onah. The effect of iron dopants concentration on the optical properties of SILAR deposited ZnSFe thin films for solar thermal applications. ***Indian J. Eng***. 2023; 20, e21ije1649 doi: https://doi.org/10.54905/disssi/v20i53/e21ije1649

[11] CC Uhuegbu. Spectral Selective Properties and Possible Applications of Iron Zinc Sulphide Ternary Thin Film. *J. Basic. Appl. Sci. Res.* 2011; 1(4), 307-311.

[12] SS Dhasade, JS Patil, JV Thombare and VJ Fulari. Studies on Synthesis and Characterization of Copper Sulfide Thin Films. Journal of Shivaji University (Science & Technology), 2014-2015; 41(2)

[13] VK Ashith and K Gowrish Rao. Structural and Optical Properties of ZnS Thin Films by SILAR Technique obtained by acetate Precursor. *IOP Conf Ser Mater Sci Eng.* 2018; 360, 012058. doi:10.1088/1757-899X/360/1/012058

[14] IJ Ferrer, DM Nevskaia, C Heras and C Sanchez. Preparation of n-type doped FeS_2 thin films. Solid State Commun. 1990; 74, 913.

[15] I Benesperi, R Singh, M Freitag. Copper Coordination Complexes for Energy-Relevant Applications. *Energies*. 2020; 13(9):2198. https://doi.org/10.3390/en13092198

[16] SW Shin, RR Kang, JH Yun, AV Moholkar, JH Moon, JY Lee and JH Kim. Effect of different annealing conditions on the properties of chemically deposited ZnS thin films on ITO coated glass substrates. Sol. Energy Mater. 2011; 95, 856.

[17] PP Rajbhandari, TP Dhakal and CR Westgate. Thin film Iron Pyrite synthesized by sulfurization of Iron Oxide for application in photovoltaics, *2014 IEEE 40th Photovoltaic Specialist Conference (PVSC)*, Denver, CO, USA, 2014, 2400-2403, doi: 10.1109/PVSC.2014.6925411.

[18] AV Babalola, V Oluwasusi, VA Owoeye, JO Emegha, DA Pelemo, AY Fasasi, UM Gurku, SO Alayande, S Yusuf and B Saje, Effect of tin concentrations on the elemental and optical properties of zinc oxide thin films. Heliyon 2024; 10, e23190.

[19] B Olofinjana, AC Adebisi, FO Efe, O Fasakin, KO Oyedotun, MA Eleruja, EOB Ajayi and N Manyala. Single solid source precursor route synhesis of MOCVD Cu-Cd-S thin films. Mater. Res. Express 2019; 6, 106442.

[20] JO Emegha, J Damisa, FO Efe, B Olofinjana, MA Eleruja, and SO Azi. Preparation and characterization of metal organic chemical vapour deposited copper zinc sulphide thin films using single solid source precursors, Euro. J. Mater. Sci. Eng. 2019; 4(1), 11-22. DOI: 10.36868/ejmse.2019.04.01.011.

[21] V Ciupina, G Prodan, V Jonescu, C Casapu, D Manole, D Tudoran, E Vasile and LM Oancea. Structural properties and composition analysis of Cu-Ni-Co alloy thin film. Solid State Phys. 2007; 53, 829-832.

[22] FO Efe, B Olofinjana, O Fasakin, MA Eleruja and EOB Ajayi. Compositional, structural, morphological, optical and electrical property evolutions in MOCVD Cu-Zn-S thin films prepared at different temperatures using a single solid source. J. Electron. Mater.2019; 48, 8000-13.

[23] E Elgazzar. Impact of Pd^{2+} and Sn^{4+} co-doping ZnO nanofakes toward high-performing Schottky diode based on the generation of intermediate bands within the energy gap. J Mater Sci: Mater Electron 2024; 35, 1697

[24] J Damisa, B Olofinjana, O Ebomwonyi, F Bakare and SO Azi. Morphological and optical study of thin films of CuAlS2 deposited by metal organic chemical vapour deposition technique. Mater. Res. Express 2017; 4, 1-10.

[25] JO Emegha, KE Ukhurebor, EO Nonum, TE Arijaje, E Danladi, TC Simon, Optoelectronic Properties of Chemically Synthesized Copper Cadmium Sulphide Thin Films, J. Appl. Sci. Environ. Manage. 2022; 26(3), 385-392

[26] J Damisa, JO Emegha. XRD and UV-Vis Spectroscopic Studies of Lead Tin Sulphide (PbSnS) Thin Films, Trends Sci. 2021; 18(20), 16. doi.org/10.48048/tis.2021.16

[27] DE Elete, JO Emegha, NO Nenuwe, and OW Omagbemi. Synthesis and characterization of chemical bath deposited copper doped lead sulfide thin *films. Bull. Chem. Soc. Ethiop***.** 2023; 37(5), 1237-1251

[28] SM Ho. Recent Advances in the Growth and Characterizations of SILAR Deposited Thin Films. Appl. Sci. 2022; 12, 8184. https://doi.org/ 10.3390/app12168184

[29] S Ahmad, M Ashraf, A Ahmad and DV Singh. Electronic and optical properties of semiconductor and alkali halides. Arab J. Sci. Eng. 2013; 38, 1889-1894.

[30] A. S. Hassanien, A.A. Akl, Influence of composition on optical and dispersion parameters of thermally evaporated non-crystalline $Cd_{50}S_{50-x}Se_x$. *J. Alloy Compd.* **648** (2015) 280-290.

[31] FO Efe, B Olofinjana, O Fasakin, CA Adebisi, MA. Eleruja, and TG Fabunmi, Opto-electronic properties of copper-zinc-sulfide thin films grown via metalorganic-chemical vapor deposition technique at different flow rates. Phys. Scr. 2023; 98(8), 085914. doi: 10.1088/1402-4896/ace2f8.

[32] JO Emegha, ED Elete, FO Efe and AC Adebisi. Optical and electrical properties of semiconducting ZnS thin films prepared by chemical bath deposition technique. J. Mater. Sci. Res. Rev. 2019; 4, 1- 8.

[33] PA Nwofe, KT Ramakrishna Reddy, JK Tan, I Forbes and RW Miles. Thickness dependent optical properties of thermally evaporated SnS thin films. Phys. Precedia. 2012, 25, 150-157.

[34] R Zarei Moghadam, MH Ehsani, H Rezagholipour Dizaji and MR Sazideh. Thickness dependence of structural and optical properties of CdTe films. IJMSE 2018, 15(3), 21 - 31